AD-A174 271 HIGH-SPEED PULSE TRANSMISSION ALONG A SLOW-WAVE CPW FOR 1/1
MONOLITHIC MICROW (U) TEXASUUNIV AT AUSTIN MICROWAVE
LAB C C TZUANG ET AL 19 SEP 86 MW-86-P-3
UNCLASSIFIED N00014-79-C-0553 F/G 9/5 NL

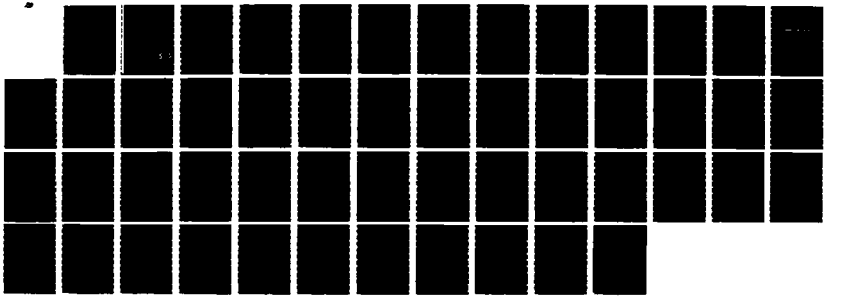

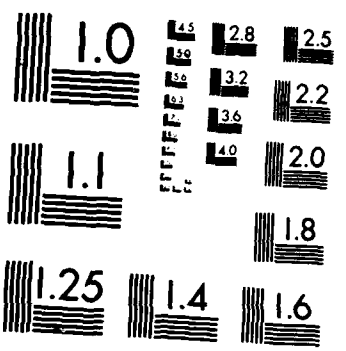

(10)

MICROWAVE LABORATORY REPORT NO. 86-P-3

HIGH-SPEED PULSE TRANSMISSION ALONG A SLOW-WAVE CPW FOR MONOLITHIC MICROWAVE INTEGRATED CIRCUITS

TECHNICAL REPORT

CHING-KUANG C. TZUANG AND TATSUO ITOH

SEPTEMBER 19, 1986

OFFICE OF NAVAL RESEARCH

CONTRACT NO. N00014-79-C-0553

UNIVERSITY OF TEXAS

DEPARTMENT OF ELECTRICAL ENGINEERING

AUSTIN, TEXAS 78712

APPROVED FOR PUBLIC RELEASE

DISTRIBUTION UNLIMITED

SECURITY CLASSIFICATION OF THIS PAGE (When Data Entered)

REPORT DOCUMENTATION PAGE	READ INSTRUCTIONS BEFORE COMPLETING FORM
1. REPORT NUMBER: Microwave Laboratory Rept. No. 86-P-3	2. GOVT ACCESSION NO. / 3. RECIPIENT'S CATALOG NUMBER
4. TITLE (and Subtitle): High-Speed Pulse Transmission Along a Slow-Wave CPW for Monolithic Microwave Integrated Circuits	5. TYPE OF REPORT & PERIOD COVERED: Technical Report
	6. PERFORMING ORG. REPORT NUMBER
7. AUTHOR(s): Ching-Kuang C. Tzuang and Tatsuo Itoh	8. CONTRACT OR GRANT NUMBER(s): N00014-79-C0553
9. PERFORMING ORGANIZATION NAME AND ADDRESS: Dept. of Electrial & Computer Engineering, University of Texas at Austin, Austin, TX 78712	10. PROGRAM ELEMENT, PROJECT, TASK AREA & WORK UNIT NUMBERS
11. CONTROLLING OFFICE NAME AND ADDRESS	12. REPORT DATE: Sept. 19, 1986
	13. NUMBER OF PAGES: 42
14. MONITORING AGENCY NAME & ADDRESS (if different from Controlling Office)	15. SECURITY CLASS. (of this report)
	15a. DECLASSIFICATION/DOWNGRADING SCHEDULE

16. DISTRIBUTION STATEMENT (of this Report)

This document has been approved for public release and sale; its distribution is unlimited.

17. DISTRIBUTION STATEMENT (of the abstract entered in Block 20, if different from Report)

18. SUPPLEMENTARY NOTES

19. KEY WORDS (Continue on reverse side if necessary and identify by block number)

Picosecond pulse, Coplanar waveguide, slow-wave, monolithic microwave integrated circuit, mode matching method, Fourier transform

20. ABSTRACT (Continue on reverse side if necessary and identify by block number)

Very high-speed picosecond range pulse transmission along a coplanar wave guide (CPW) integrated in a monolithic microwave integrated circuit (MMIC) is analyzed in the time domain, changing the input excitations, conductivity of the epitaxial layer, and terminating conditions. The time domain waveform is obtained by inverse discrete Fourier transform (IDFT) of the frequency domain data, namely, complex characteristic impedance and propagation constant. The full wave mode-matching method (MMM) is employed to analyze the dispersion of the CPW. A simple wide band matching scheme is found to be effective to make the slow-wave

DD FORM 1 JAN 73 1473 EDITION OF 1 NOV 65 IS OBSOLETE
S/N 0102-014-6601

SECURITY CLASSIFICATION OF THIS PAGE (When Data Entered)

20. (cont'd)

CPW a viable circuit element in applications such as a delay line or an interconnnection line. Knowing the device processing data and physical dimensions, a designer should benefit from the present analysis that simulates the transmission of a very high-speed pulse on an MMIC CPW under various terminations.

MICROWAVE LABORATORY REPORT NO. 86-P-3

HIGH-SPEED PULSE TRANSMISSION ALONG A SLOW-WAVE CPW FOR MONOLITHIC MICROWAVE INTEGRATED CIRCUITS

TECHNICAL REPORT

CHING-KUANG C. TZUANG AND TATSUO ITOH

SEPTEMBER 19, 1986

OFFICE OF NAVAL RESEARCH

CONTRACT NO. N00014-79-C-0553

UNIVERSITY OF TEXAS

DEPARTMENT OF ELECTRICAL ENGINEERING

AUSTIN, TEXAS 78712

APPROVED FOR PUBLIC RELEASE

DISTRIBUTION UNLIMITED

High-Speed Pulse Transmission along a Slow-Wave CPW for Monolithic Microwave Integrated Circuits

Abstract

Very high-speed picosecond range pulse transmission along a coplanar wave guide (CPW) integrated on a monolithic microwave integrated circuit (MMIC) is analyzed in the time domain, changing the input excitations, conductivity of the epitaxial layer, and terminating conditions. The time domain waveform is obtained by inverse discrete Fourier transform (IDFT) of the frequency domain data, namely, complex characteristic impedance and propagation constant. The full wave mode-matching method (MMM) is employed to analyze the dispersion of the CPW. A simple wide band matching scheme is found to be effective to make the slow-wave CPW a viable circuit element in applications such as a delay line or an interconnection line. Knowing the device processing data and physical dimensions , a designer should benefit from the present analysis that simulates the transmission of a very high-speed pulse on an MMIC CPW under various terminations.

TABLE OF CONTENTS

LIST OF FIGURES

CHAPTER 1 : Introduction

The advance in monolithic microwave integrated circuits (MMIC's) and picosecond optoelectronic devices has continuously improved the switching speed of the active devices and pushed the real time high-speed signal processing into the picosecond range [1,2]. Operating at speed higher than gigabits per second, the conventional lumped capacitance approximation of an interconnection line in an MMIC can not be used for accurate analysis on pulse transmission. Instead, microwave considerations are required in the logic, circuit, and layout of very high-speed integrated circuits[3]. In addition to the propagation delay, it is important to know the actual signal waveform after its propagation along an interconnection line which connects both the source and the load, since the waveform parameters such as rise time, fall time, settling time, overshoot and undershoot play a fundamental role for the success of a very high-speed digital or wideband analog integrated circuit. The signal degradations stemming from both the dispersive characteristics of a coplanar waveguide (CPW) integrated on an MMIC and the improper terminations will be discussed in this paper.

The CPW has also become an important transmission line

element in MMIC technologies because of its easy access for the ground plane, reduction in crosstalk between adjacent transmission lines, and less radiation at discontinuities as compared to a microstrip [4,5]. When a CPW becomes part of a microcircuit, slow-wave propagation may occur. Planar metal-insulator-semiconductor (MIS) and Schottky contact CPW were examined and the existence of the slow-wave propagation was both experimentally and theoretically confirmed [6,7]. As the physical dimensions of the CPW are getting smaller, the finite conductor thickness of a CPW is no longer negligible. Therefore, it is clear that only accurate field calculations of a CPW can result in accurate simulation of an ultra high-speed narrow pulse transmission on an MIS or Schottky contact slow-wave CPW.

Historically, it was reported that severe signal degradations can occur for pulse transmission along a well matched semi-infinite lossless microstrip and a CPW for distance less than 1 cm [8,9,10]. The case of pulse transmission with possible existence of slow-wave propagation was reported in [11,12,13]. However, no detailed studies have been reported so far. The purpose of this paper is to present detailed time domain analyses of pulse transmissions on an MIS or Schottky contact CPW integrated in a microcircuit under various kinds of input excitations and arbitrary combinations of source and load

terminations. A hybrid TE and TM full wave analysis based on the mode-matching method is applied to our model shown in Figure 1.1. Once the complex propagation constant is obtained, the field distributions inside a slow-wave CPW are known. The Poynting power and the current flowing on the surface of the signal (or center) conductor of a CPW can be obtained by integrations. This leads to the determination of the complex characteristic impedance based on the power-current definition. The validity of the accuracy of the characteristic impedance defined by the power-current definition is checked against that obtained by the power-voltage definition based on the spectral domain analysis (SDA). After the accuracy is confirmed, the inverse discrete Fourier transform (IDFT) is invoked to convert the frequency domain data into time domain equivalents. It is found that an impedance matching scheme can be useful in making a slow-wave CPW a good interconnection line or a delay line with very little degradation on the propagating waveform.

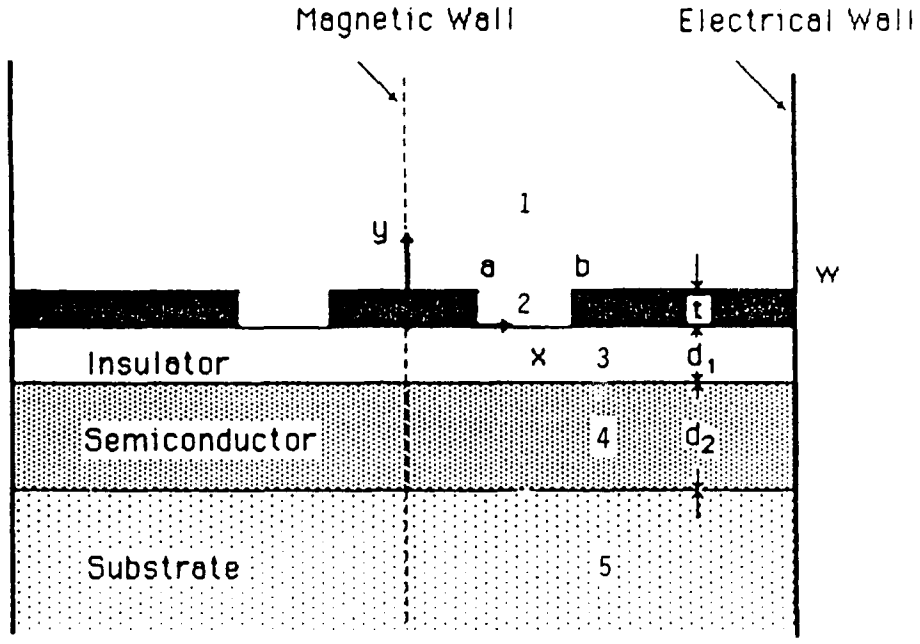

Figure 1.1 The slow-wave coplanar waveguide model.

CHAPTER 2 : Model and Method of Analysis

A. the Physical Model

The slow-wave CPW model shown in Figure 1.1. was used for the analysis. The coplanar waveguide with finite conductor thickness is located on top of a layered structure. It consists of metal, insulator (or depletion region for Schottky contact), semiconducting layer (or epitaxial layer), and semi-insulating substrate. By setting the conductivity of the semiconductor layer to zero, Figure 1.1 may represent a conventional lossless CPW. This model is general enough to analyze most CPW's integrated in MMIC. By knowing the integrated circuit processing data and physical dimensions , one should be able to compute the time domain pulse waveform propagating on such a CPW.

B. Frequency Domain Analysis

The mode-matching method which has been widely used to analyze various waveguide structures [14,15] was applied to the frequency domain analysis of the slow-wave CPW shown in Figure 1.1. The technique itself does not result in a unique formulation for the same problem. Instead, many possible formulations can

yield the same solution for the propagation constant. Because of the even symmetry for the propagating mode of interest, a magnetic wall is placed at the center of the guide. Electric walls are placed at far distance to simplify the analysis [7]. The modal field expansions in each region shown in Figure 1 can be expressed in terms of TE-to-y and TM-to-y Hertzian potentials written as:

$$\vec{A} = \vec{e}_y \psi(x,y) e^{-j\gamma z} \qquad \text{TM-to-y}$$

$$\vec{F} = \vec{e}_y \phi(x,y) e^{-j\gamma z} \qquad \text{TE-to-y}$$

$$\vec{E} = -\nabla \times \vec{F} - j\omega\mu_o \vec{A} + \frac{1}{j\omega\varepsilon_o\varepsilon_R} \nabla(\nabla\cdot\vec{A})$$

$$\vec{H} = \nabla \times \vec{A} - j\omega\varepsilon_o\varepsilon_R \vec{F} + \frac{1}{j\omega\mu_o} \nabla(\nabla\cdot\vec{F})$$

$$\varepsilon_R = \varepsilon_r - j\,\frac{\sigma}{\omega\varepsilon_o} \qquad (1)$$

,where ε_r and σ are the relative dielectric constant and the conductivity of the dielectric material, respectively.

For instance, the potential functions in region 1 are:

$$\psi^1(x,y) = \sum_{m=1}^{M} A_m \cos(\beta_m x) e^{-\alpha_{1m}(y-t)}$$

$$\Phi^1(x,y) = \sum_{m=1}^{M} B_m \text{sub}(\beta_m x) e^{-\alpha_{1m}(y-t)}$$

$$\beta_m = \frac{(2m-1)\pi}{2W} \; ; \; \alpha_{1m}^2 - \gamma^2 - \beta_m^2 + \omega^2 \mu_o \varepsilon_o \varepsilon_{R1} = 0 \qquad (2)$$

In region 2, the potential functions are:

$$\psi^2(x,y) = \sum_{n=2}^{N} \sin[\beta_{2n}(x-a)]\{C_n \sin(\alpha_{2n} y) + \tilde{C}_n \cos(\alpha_{2n} y)\}$$

$$\Phi^2(x,y) = \sum_{n=1}^{N} \cos[\beta_{2n}(x-a)]\{D_n \sin(\alpha_{2n} y) + \tilde{D}_n \cos(\alpha_{2n} y)\}$$

$$\beta_{2n} = \frac{(n-1)\pi}{b-a} \; ; \; \alpha_{2n}^2 + \beta_{2n}^2 + \gamma^2 = \omega^2 \mu_o \varepsilon_o \varepsilon_{R2} \qquad (3)$$

The potential functions in regions 3 through 5 can be derived in a similar way such that they satisfy the boundary conditions imposed by the radiation condition and by both magnetic wall and electric walls.

Summarize the coefficients in all regions :

Region	Coefficients		
1	A_m	B_n	
2	$C_n\tilde{C}_n$	$D_n\tilde{D}_n$	
3	$E_m\tilde{E}_m$	$F_m\tilde{F}_m$	
4	$G_m\tilde{G}_m$	$H_m\tilde{H}_m$	
5	I_n	J_m	(n:1~N) (m:1~M)

(4)

By matching the adjacent tangential fields in regions 3 through 5 and applying the orthogonality relationships between potential functions, only Em and Fm remain. This means that the coefficients in regions 3 through 5 can be expressed in terms of Em and Fm only. Next, we match the adjacent tangential fields in regions 1 through 3. The boundary conditions at the interfaces of these regions are:

$$\text{At } y=t,\ H_{1t}=H_{2t},\ 0 < x < b \tag{5}$$

$$E_{1t}=E_{2t},\ a < x < b \tag{6}$$

$$E_{1t}= 0\ ,\ 0 \leq x \leq a,\ b \leq x \leq w \tag{7}$$

At y=0, the boundary conditions are similar to equations (5) through (7). As the boundary conditions (6) and (7) are satisfied simultaneously, Am and Bm (Em and Fm) can be expressed in terms of Cn, $\tilde{C}_n$, Dn, and $\tilde{D}_n$. If the boundary condition (5) is

satisfied, Cn, $\tilde{C}n$, Dn, and $\tilde{D}n$ can be expressed in terms of Am and Bm (Em and Fm). Finally, a homogeneous matrix equation of dimension (2N - 1) by (2N -1) can be derived.

$$\left[\begin{array}{c|c} P_{mn} & Q_{mn} \\ \hline R_{mn} & S_{mn} \end{array}\right] \cdot \left[\begin{array}{c} C_2 \\ \vdots \\ C_n \\ \hline \tilde{D}_1 \\ \vdots \\ \tilde{D}_n \end{array}\right] = 0 \qquad (AX = 0) \tag{8}$$

The expressions for Pmn(γ), Qmn(γ), Rmn(γ), and Smn(γ) are obtained from the equations (A-1) and (A-2) shown in Appendix. To obtain a nontrivial solution for the column vector X of the equation (8), the unknown coefficients of Cn and $\tilde{D}n$, the determinant of the matrix A has to be zero. The real and imaginary parts of correspond to the slow-wave factor (λ_o/λ_g) and the attenuation constant, respectively.

C. Complex Characteristic Impedance

Once the complex propagation constant γ is obtained, the unknown field coefficients C_n and $\tilde{D}_n$ are found within a constant

multiplicative factor. The field distributions in each region are solved immediately. Based on the power-current definition, the characteristic impedance is expressed as

$$Z_o = \frac{\int_S \vec{E}_t \times H_t^* da}{|I_t|^2} = \frac{1}{2} \frac{\sum_{k=1}^{5} \int_{S_k} (E_{kx} H_{ky}^* - E_{ky} H_{kx}^*) da_k}{\left| \int_0^a (H_{3x})_{y=0} dx + \int_0^t (H_{2y})_{x=a} dy - \int_0^a (H_{1x})_{y=t} dx \right|^2} \tag{9}$$

where the subscript k denotes the subregion k and S is the cross-sectional area of the CPW.

D. Time Domain Analysis

An equivalent linear 2-port ABCD matrix representation of the CPW can be applied to derive the complex transfer function ,at a distance of z from the source, of a terminated slow-wave CPW shown in Figure 2.1 at each incremental frequency step. The transfer function can be written in terms of γ and Z_o as:

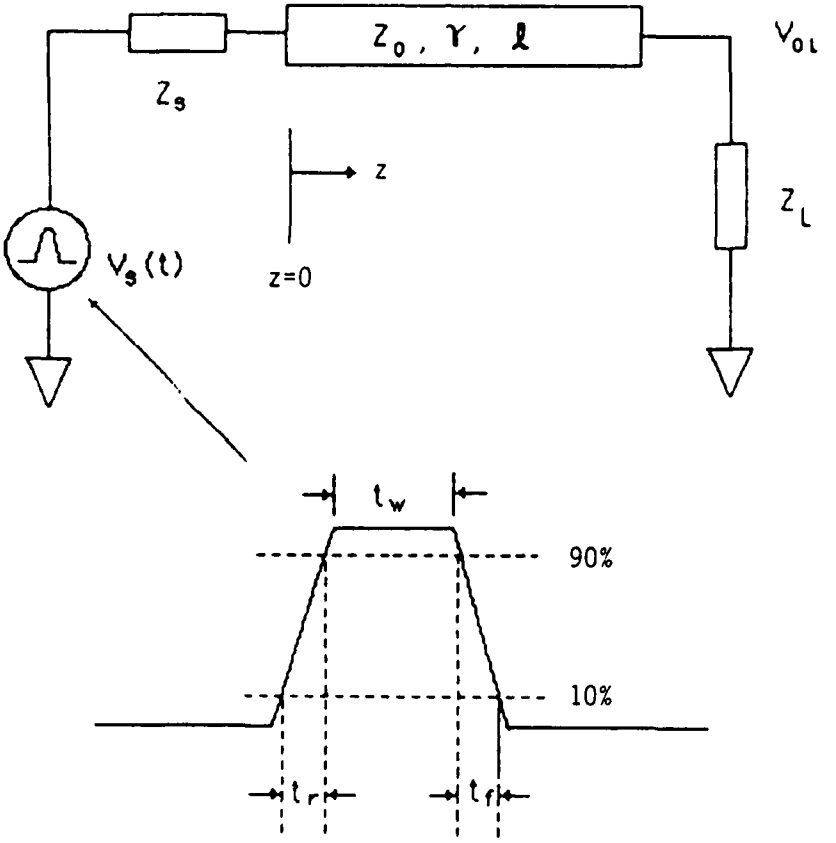

Figure 2.1 Equivalent circuit representation of a slow-wave CPW.

$$\frac{V_o(n\omega)}{V_s(n\omega)} = \frac{ZL_e(n\omega)}{\cos(\gamma z)ZL_e(n\omega)+jZ_o\sin(\gamma z)+\left(j\sin(\gamma z)ZL_e(n\omega)/Z_o+\cos(\gamma z)\right)Z_s}$$

$$ZL_e(n\omega) = \frac{\cos[\gamma(\ell-z)]Z_L + jZ_o\sin[\gamma(\ell-z)]}{j\sin[\gamma(\ell-z)]Z_L/Z_o + \cos[\gamma(\ell-z)]} \qquad (10)$$

,where n is an integer.

The corresponding time domain function is recovered by means of a standard inverse discrete Fourier transform(IDFT) procedure. Both rectangular pulse of finite rise and fall times and Gaussian pulse of finite width are applied to analyze time domain waveforms. Note that the case for a lossless, well-matched, and semi-infinitely long transmission line is a special case obtained by setting $Z_L = Z_o$ and Zs = 0 in equation (10).

CHAPTER 3 : Frequency-Domain Solutions

Figures 3.1-(a) and 3.1-(b) are the plots of the normalized propagation constant and the characteristic impedance obtained by both MMM and SDA for infinitely thin conductors, respectively. The discrepancy of the propagation constant shown in Figure 3.1-(a) between two methods is contributed by the finite conductor thickness of the CPW analyzed by the MMM. If the conductor thickness becomes one hundredth of the half center strip width a, the propagation constants obtained by both MMM and SDA agree to within .5 %. It is interesting to see the discrepancy of the characteristic impedance at higher frequency among the power-current and the power-voltage definitions obtained by MMM and SDA, respectively. We may need to incorporate more basis functions than only two terms currently used in the SDA code available for our analysis when the CPW under study starts to depart from the quasi-TEM mode of propagation, since the quasi-TEM mode approximation is no longer held at higher frequency and the voltage defined by the integration across the slot is not a good approximation. In contrast, the current which can be well defined becomes smaller when the CPW is away from the quasi-TEM mode. Therefore the characteristic impedance defined by the power-current definition is higher at higher frequency.

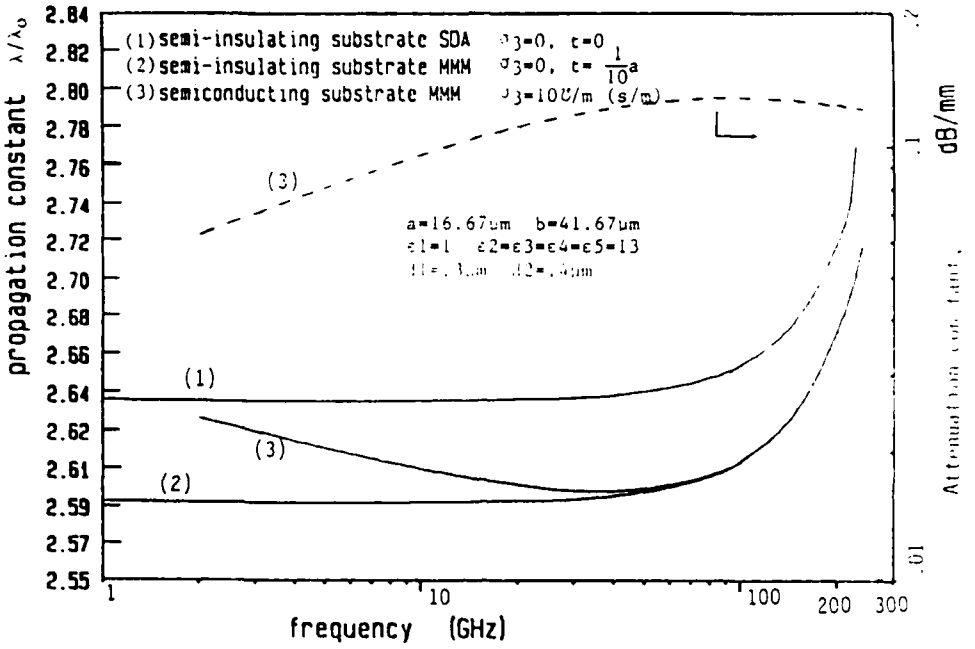

Figure 3.1-(a) Propagation constant versus frequency.

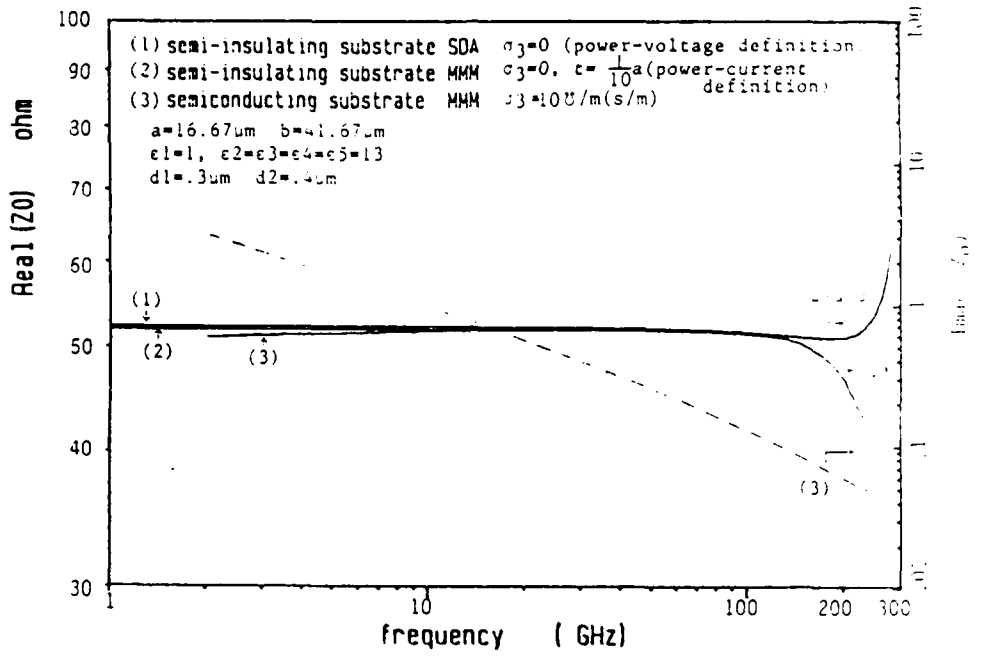

Figure 3.1-(b) Real and imaginary parts of the characteristic impedance versus frequency.

Figure 3.1 Propagation constant and characteristic impedance versus frequency obtained by both MMM and SDA.

Nevertheless these plots indicate an upper frequency limit for a CPW that still supports the quasi-TEM mode. In the present case, we set the upper frequency limit to be approximately 270 GHz according to the judgments from Figure 3.1-(b) and use the same physical dimensions of the CPW for later time domain calculations.

Figure 3.1 also shows the case with a thin semiconducting epitaxial layer which has finite resistivity of 10 Ω-cm corresponding to $10^{14}/cm^3$ n-type GaAs substrate doping [16].

Another slow-wave CPW structure with smaller dimensions is analyzed. The results are shown in Figure 3.2 for both slow-wave factor and attenuation constant versus frequency. The physical dimensions are chosen to comply with the current integrated circuit technology. The real and imaginary parts of the characteristic impedance are show in Figure 3.3. Note that the imaginary part of the characteristic impedance is divided by a factor shown in Figure 3.3 and has unit of femto farad (fF). In this way, a simple complex impedance matching technique can be derived.

A thorough check on the solutions of the field components is performed and the results are shown in Figures 3.4-(a), 3.4-(b), 3.4-(c), and 3.4-(d), respectively. The tangential electric

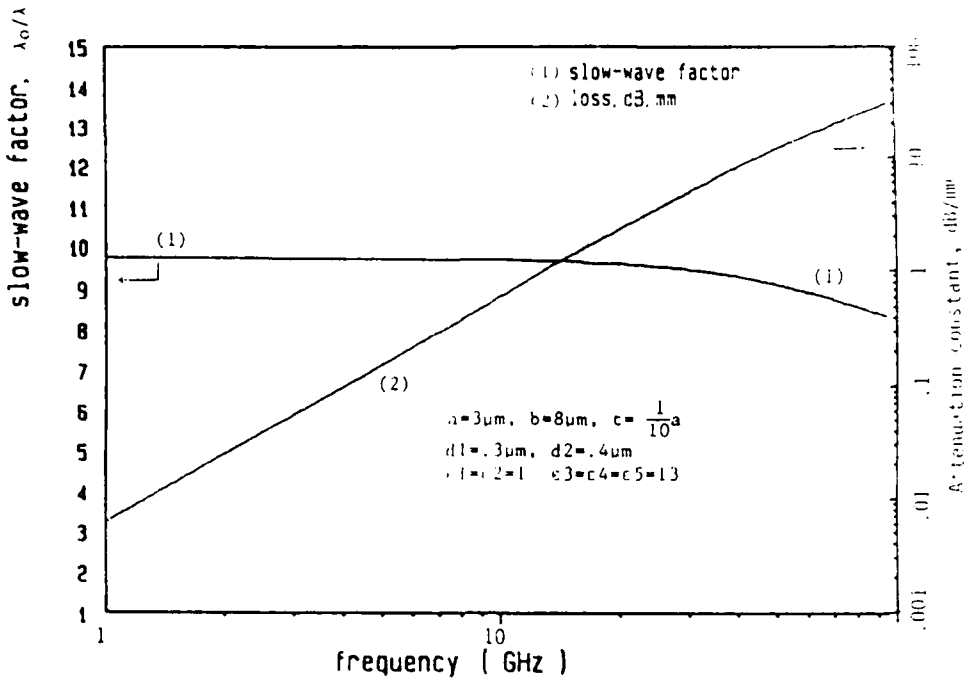

Figure 3.2 Slow-wave factor and attenuation constant for a CPW model.

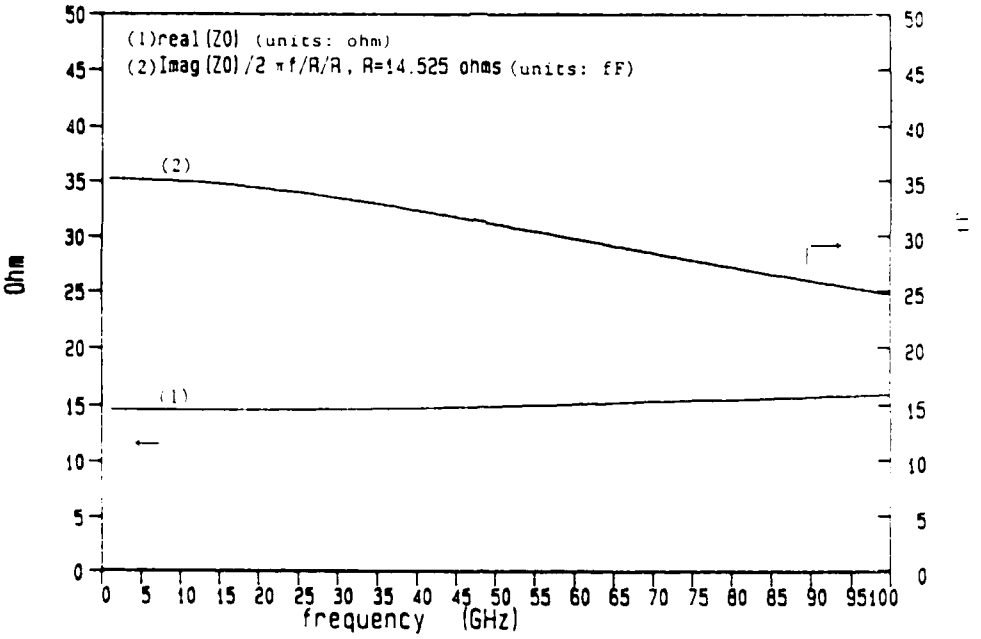

Figure 3.3 Real and imaginary parts of the characteristic impedance versus frequency for the same CPW with dimensions shown in Figure 3.2.

$|E_Y|$ Relative scale

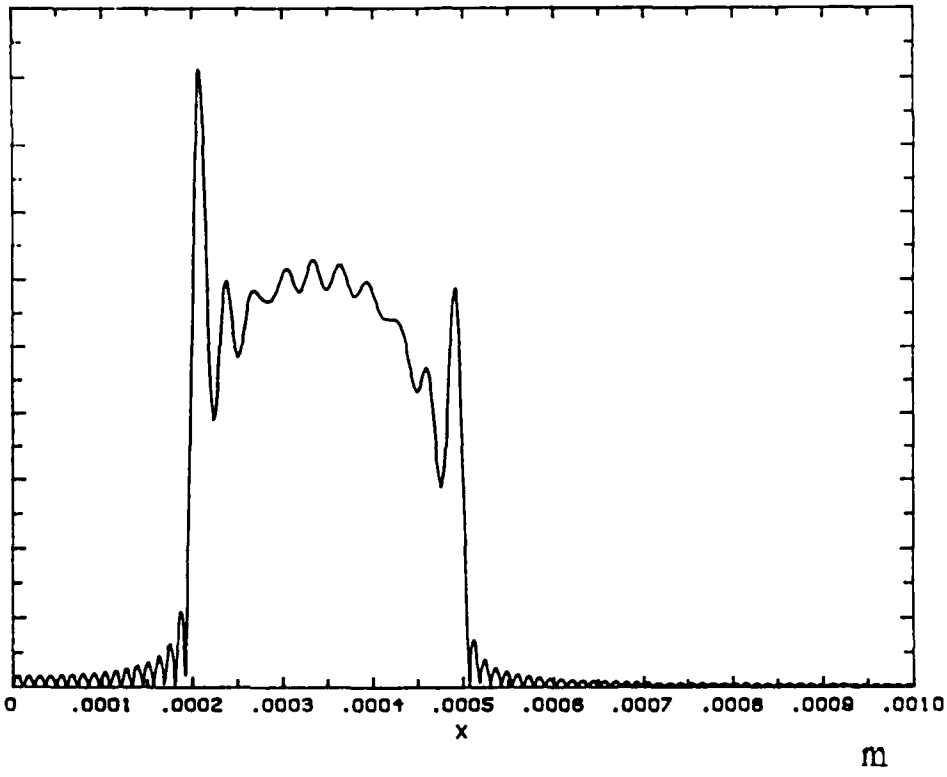

$|E_X|$ at y=T versus x along x-axis

A=0.2mm B=0.5mm W=1.7999mm
D1=0.4μm D2=1μm D3=1mm
$\sigma 4=1.82\times10^{4}$ S/m
$\epsilon_r 1=\epsilon_r 2=1.0$ $\epsilon_r 3=8.5$ $\epsilon_r 4,5$ =13.0
M=150 N=25

Figure 3.4-(a)

Relative scale

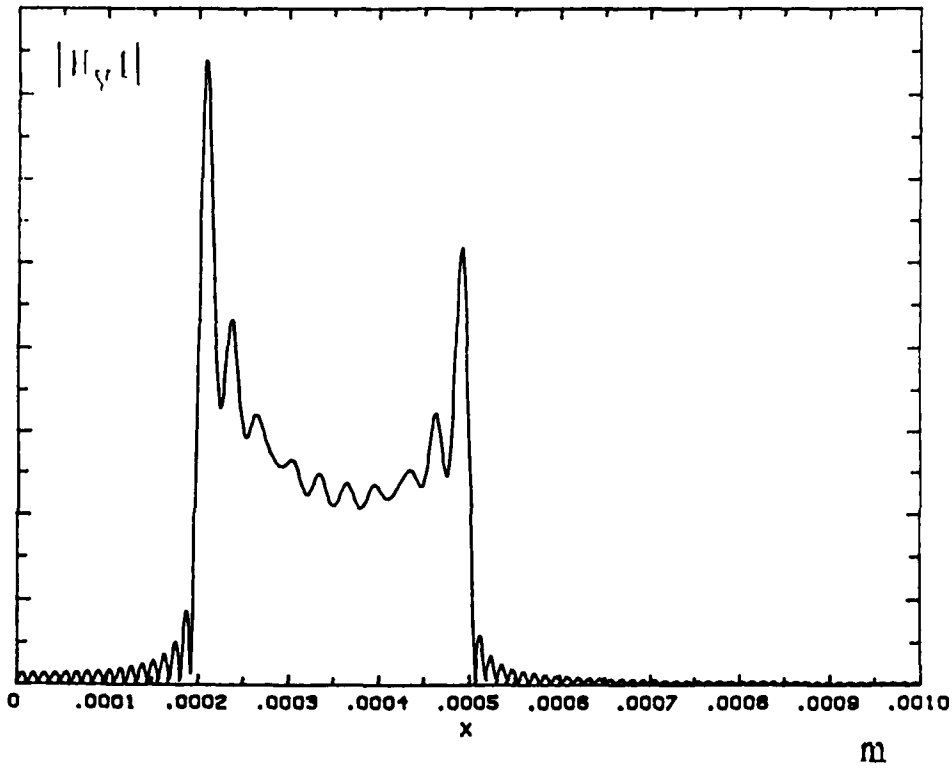

$|H_y 1|$ at y=T versus x along x-axis

A=0.2mm B=0.5mm W=1.7999mm
D1=0.4μm D2=1μm D3=1mm
$\sigma 4=1.82\times10^{4}$ S/m
$\epsilon_r 1=\epsilon_r 2=1.0$ $\epsilon_r 3=8.5$ $\epsilon_r 4,5$ =13.0
M=150 N=25

Figure 3.4-(b)

Relative scale

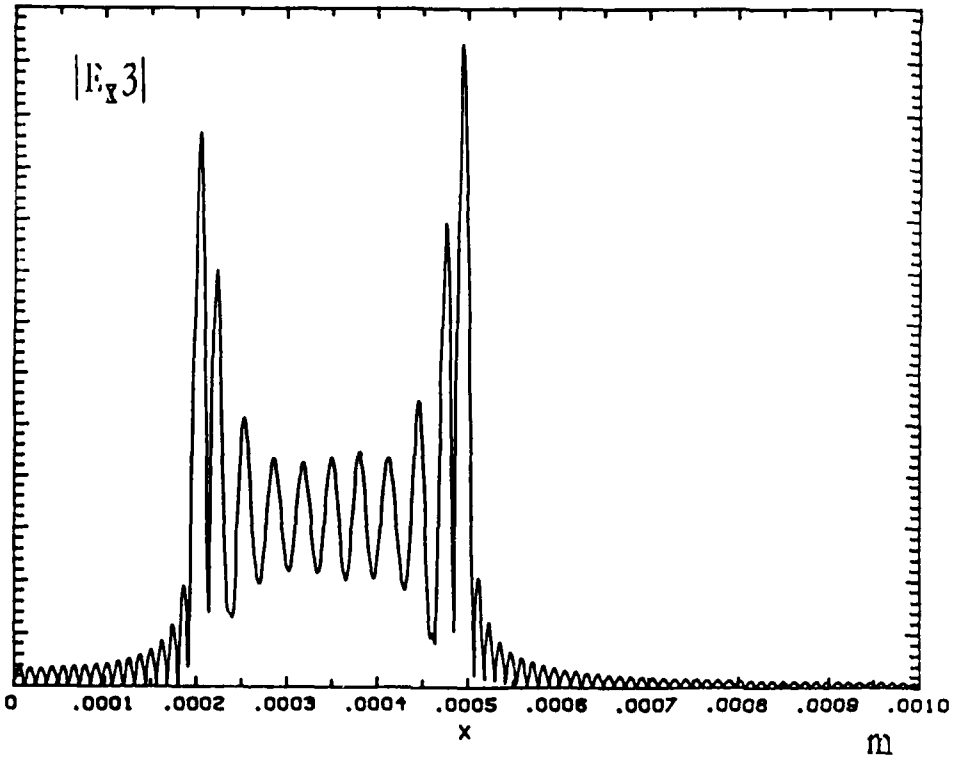

$|E_x3|$ at y=0 versus x along x-axis

A=0.2mm B=0.5mm W=1.7999mm
D1=0.4μm D2=1μm D3=1mm
$\sigma 4=1.82\times10^{4}$ S/m
$\epsilon_r1=\epsilon_r2=1.0$ $\epsilon_r3=8.5$ $\epsilon_r4,5$ =13.0
M=150 N=25

Figure 3.4-(c)

Relative scale

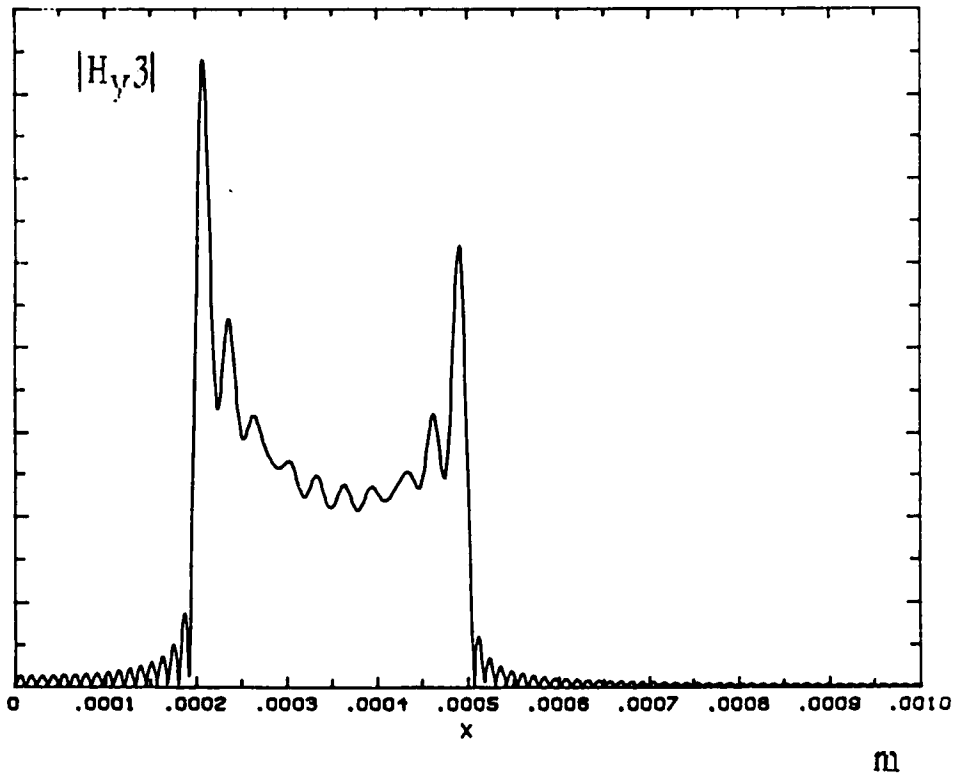

$|H_y3|$ at y=0 versus x along x-axis

A=0.2mm B=0.5mm W=1.7999mm
D1=0.4μm D2=1μm D3=1mm
$\sigma 4 = 1.82 \times 10^4$ S/m
$\epsilon_r 1 = \epsilon_r 2 = 1.0$ $\epsilon_r 3 = 8.5$ $\epsilon_r 4,5 = 13.0$
M=150 N=25

Figure 3.4-(d)

fields and the normal magnetic fields vanish as expected on the electric conductors with relatively small residues that result from the MMM employing finite expansion terms. Note also that the magnitude of the field components shown in these figures has a peak at the edge of the conductor. In exact field solutions without numerical approximations, a singularity must exist for electromagnetic field near the edge of the conductor.

CHAPTER 4 : Time-Domain Results

When a slow-wave CPW is excited by a rectangular pulse of 80 ps rise and fall times (measured by 10-90 percent rise or fall) and 300 ps wide with zero source impedance and a 10 fF load, a damped oscillatory output waveform is observed in Figure 4.1. Figure 4.1 is obtained by means of IDFT that converts the frequency domain data of Figures 3.2 and 3.3 from .1 GHz to 20 GHz at .1GHz incremental frequency step. When the output load capacitance(CL) is increased from 10 fF to 80 fF the output waveform is almost identical. This fact suggests that the output loading has little effects on the oscillation and the slow-wave CPW itself has inductive, capacitive and resistive components. From the circuit point of view, it is not surprising that the oscillation occurs since there exists a reactive (or positive imaginary) part of the complex characteristic impedance shown in Figure 3.3 for the CPW analyzed. As the transient voltage waveform is excited at the input end of the CPW, the spike will occur just like an inductor will do. Once the input excitation is settled to a DC voltage, the slow-wave CPW has to reach to the final steady state in a damped oscillation manner because the slow-wave propagation of this type usually exhibits a large capacitance in the low frequency limit [17] and the CPW itself is

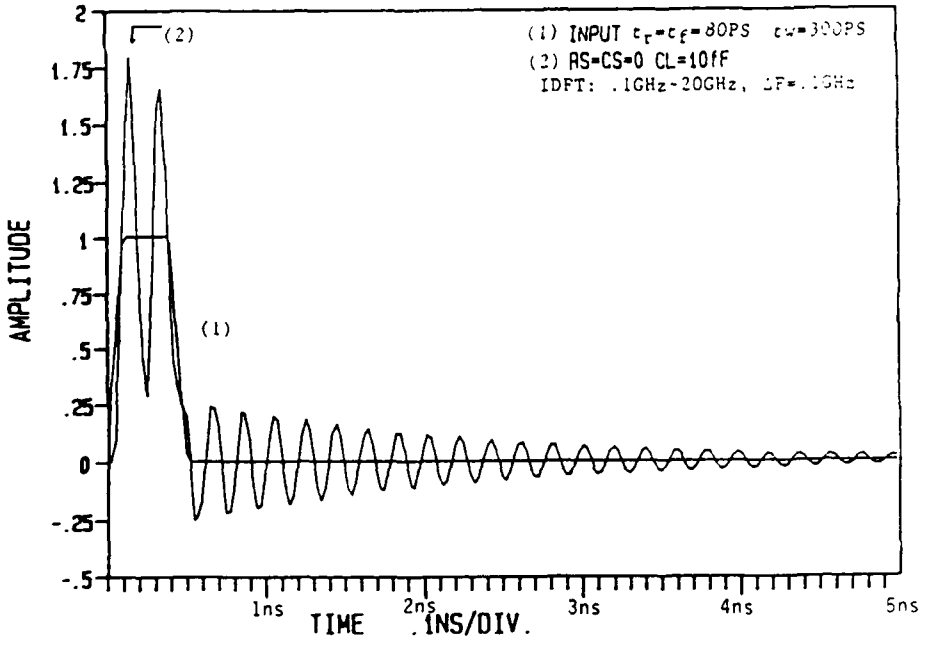

Figure 4.1 Transient excitation of a slow-wave CPW with the frequency domain data shown in Figure 3.3 with a short-circuited input and a capacitive load. l=1.5 mm

lossy as shown in Figure 3.2.

To make the slow-wave CPW a useful MMIC element it requires a good wideband matching circuit. It can be demonstrated that if either source or load impedance is designed to be a complex conjugate of the complex characteristic impedance (Z_o) of the CPW, most of the oscillations associated with the transient input excitation can be suppressed. In this way, a simple parallel RC network can be applied as a matching network. After a few algebraic manipulations under the assumption that the imaginary part of the impedance of the parallel RC network is small, one obtains $X = \omega R^2 C$, where X and R are the imaginary and real parts of the complex characteristic impedance, respectively. (ω is the angular frequency.) The curve (2) of Figure 3.3 indicates that the normalized X is almost constant for frequency up to 20 GHz and suggests this is a good choice for C.

Under the matched source and load terminations, Figure 4.2 shows that the rectangular pulse can propagate 8 cm with little degradation and is delayed by approximately 2.6 ns.

Under the unmatched terminations, the output waveform can have overshoot or undershoot with some ringing(ripple) superimposed on top of it as shown in Figure 4.3-(a) [13]. When the input source impedance is terminated by the matched load

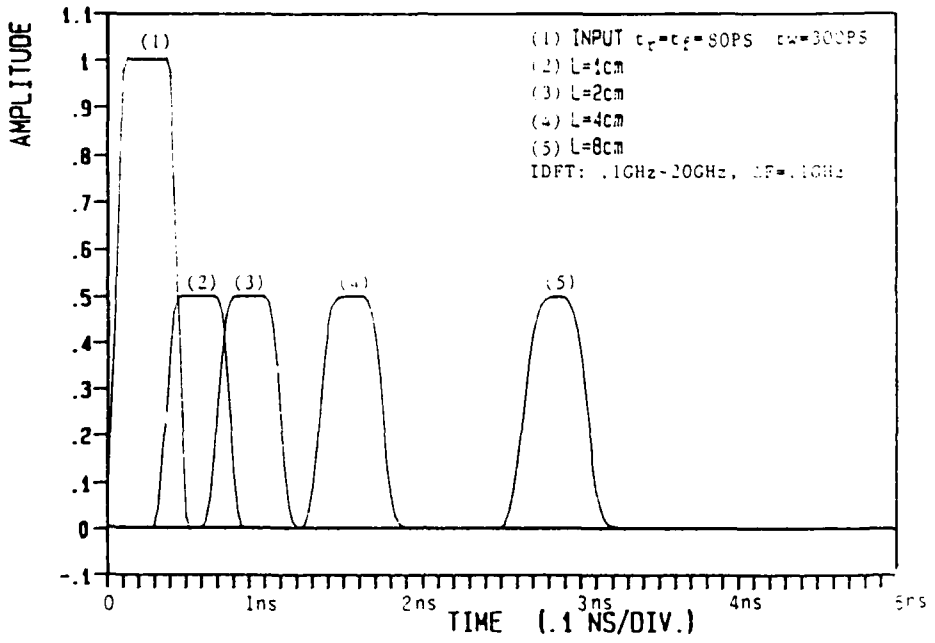

Figure 4.2 Transient pulse waveform with matched source and load terminations for CPW's with lengths ranging from 1 cm to 8 cm.

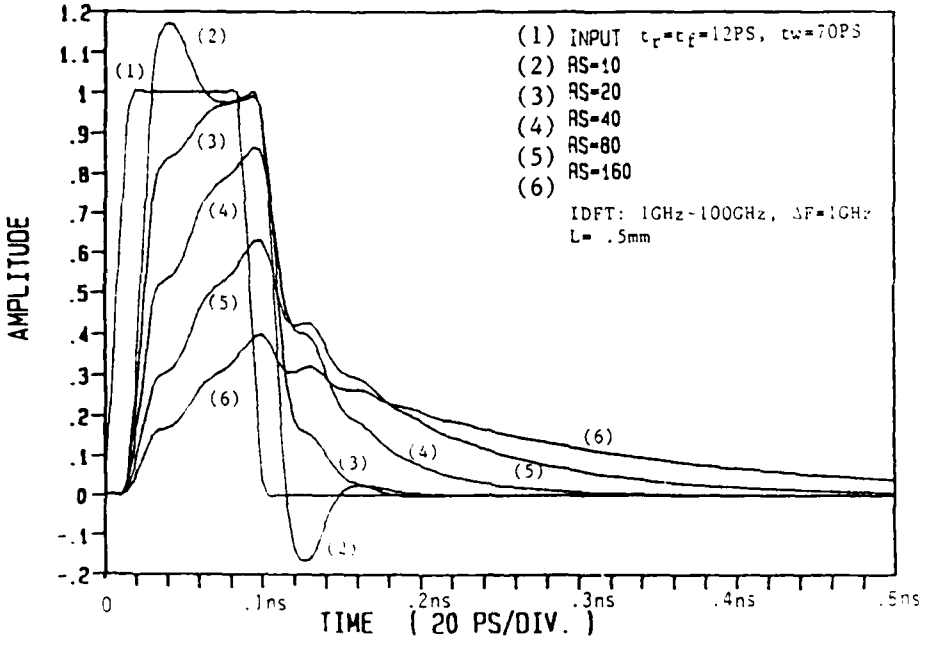

Figure 4.3-(a) Transient pulse excitations with a resistive source and a capacitive load terminations.

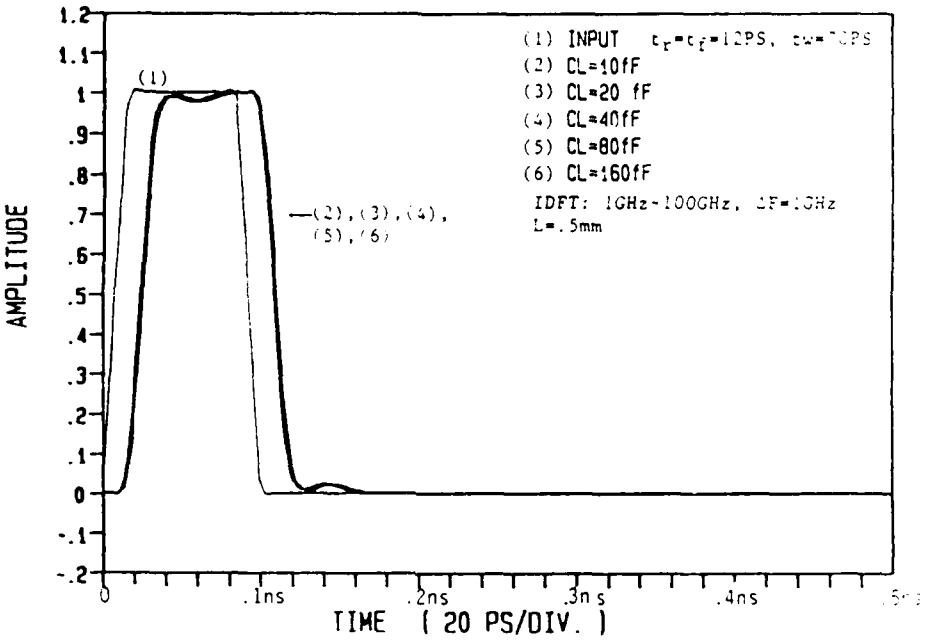

Figure 4.3-(b) Transient pulse excitations with a matched source and a capacitive load terminations.

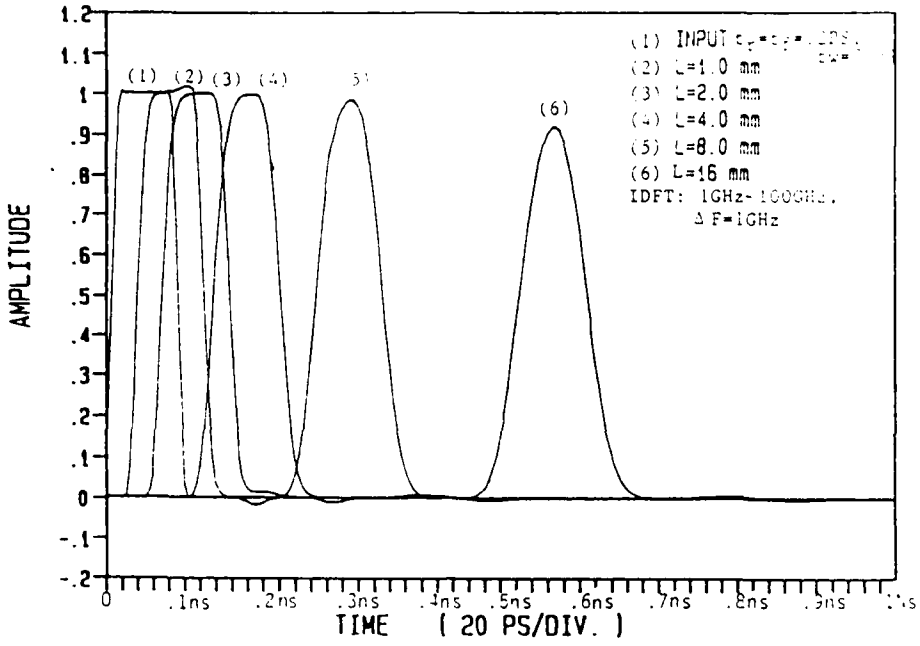

Figure 4.3-(c) Transient pulse excitations with a short-circuited source and a matched load terminations.

Figure 4.3 Transient pulse excitations on a slow-wave CPW with the frequency domain data shown in Figures 3.2 and 3.3.

described in the previous section, the output waveform has very little degradation for driving output capacitive loads up to 160 fF as shown in Figures 4.3-(b). Figure 4.3-(c) displays the pulse dispersion for different lengths of the CPW with zero (shorted) source impedance and a matched output load. Figure 4.4 shows the propagation of a Gaussian pulse of 15 ps wide at different locations of the CPW with a matched output load and either a shorted or a matched input source termination.

The GaAs MESFET is often fabricated on a thin epitaxial layer with resistivity in the order of 10 Ω-cm corresponding to $10^{14}/cm^3$ n-type doping concentrations. The results shown in curves (3) of Figures 3.1-(a) or 3.1-(b) actually correspond to such a case. These data imply that there exists no slow-wave mode or mode transition in the structure under analysis since the imaginary part of the complex characteristic impedance is very small and is closer to zero at higher frequencies. Figure 4.5, obtained by converting the frequency domain data shown in Figures 3.1-(a) and 3.1-(b) into the time domain waveform, compares the results of a Gaussian pulse of 5 ps wide observed at 1 cm and 2 cm from the source end for substrate with and without semiconducting layer. In this CPW structure, the effect of the semiconducting layer with small conductivity or low doping

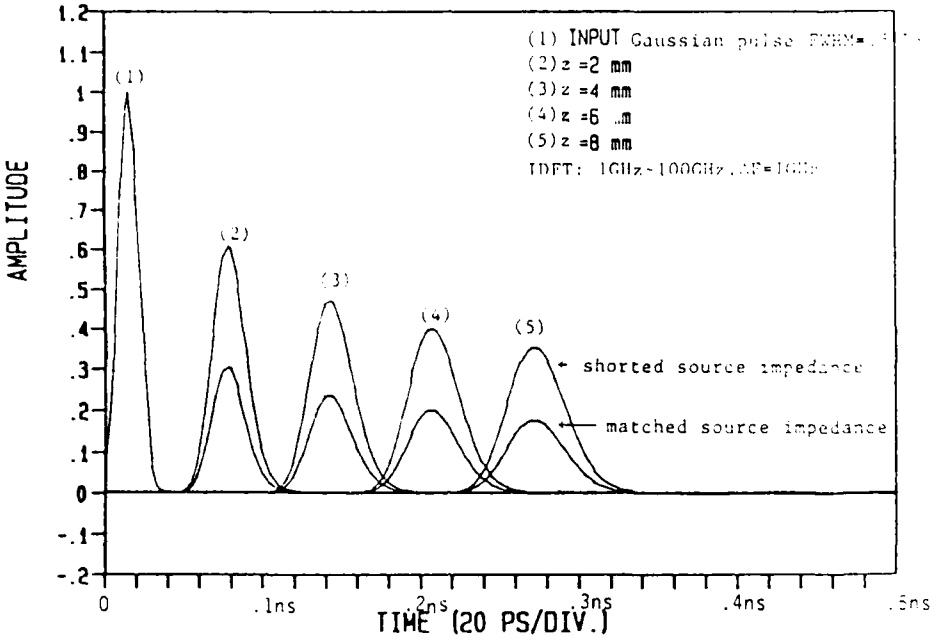

Figure 4.4 Transient Gaussian pulse excitations with a matched output load and a matched source terminations for a 10 mm long CPW with the frequency domain data shown in Figures 3.2 and 3.3.

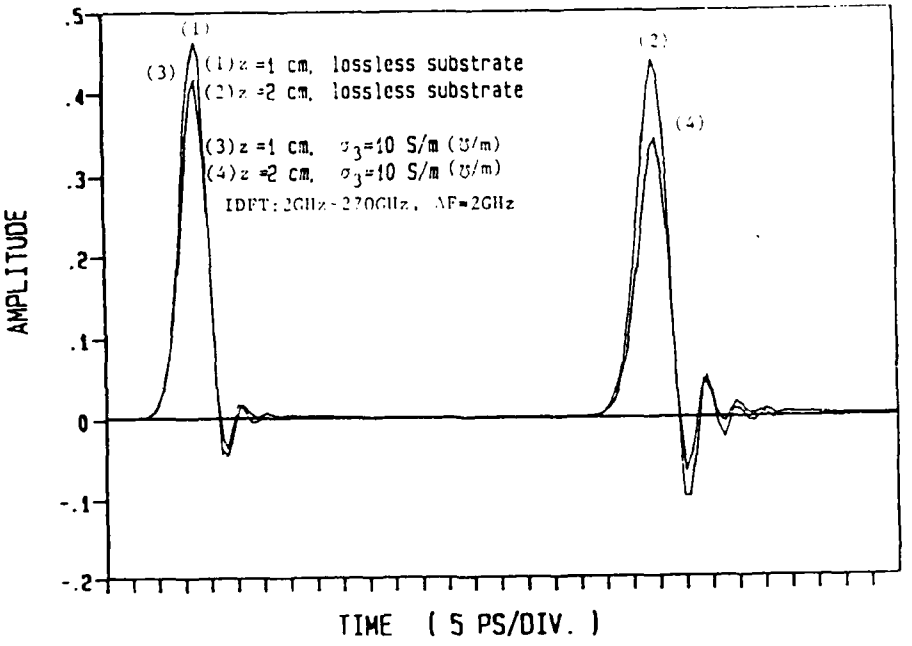

Figure 4.5 Gaussian pulse transmission along CPW's under matched terminations with and without semiconducting layer at different locations of the CPW's.

concentration attenuates the pulse waveform and does not alter the shape of the pulse waveform. Similar waveforms are also reported in [8,9,10] for the cases of a microstrip and a CPW.

CHAPTER 5 : Conclusions

Time domain response of picosecond pulse transmission along a slow-wave MIS or Schottky contact CPW is presented. The severe drawbacks such as overshoot, undershoot, and ringing in applying the slow-wave CPW [12,13] are eliminated almost entirely by an appropriate wideband impedance matching technique proposed in this paper. As a result, a slow-wave CPW can be a useful interconnection line or a delay line in MMIC's. All of these applications are analyzed separately with examples in the time domain. We may anticipate other slow-wave structures such as an MIS microstrip and a coupled microstrip should exhibit similar properties found in this paper. The theoretical approach presented in this paper proves to be a versatile tool for the solutions of very high-speed pulse transmission on an MMIC CPW.

APPENDIX

$$\sum_{m=1}^{M}\sum_{n'=2}^{N}\{R5(m,n)R1(m,n')+R6(m,n)R3(m,n')\}\cos(\alpha_{2n'}t)C_{n'}$$

$$-\sum_{m=1}^{M}\sum_{n'=2}^{N}\frac{\sin(\alpha_{2n'}t)}{\frac{(b-a)}{4}W(\omega\mu_o\gamma^2+\omega\varepsilon_o\beta_{2n'}^2)}[R5(m,n)R1(m,n')+R6(m,n)R3(m,n')]$$

$$\cdot\{\sum_{m'=1}^{M}\sum_{P=2}^{N}[(\gamma R\acute{5}(m',n')-\beta_{2n'}R\acute{7}(m',n')R1(m',p)$$

$$+(\gamma R\acute{6}(m',n')-\beta_{2n'}R\acute{8}(m',n'))R3(m',p)]C_p$$

$$+\sum_{m'=1}^{M}\sum_{P=1}^{N}[(\gamma R\acute{5}(m',n')-\beta_{2n'}R\acute{7}(m',n'))R2(m',p)$$

$$+(\gamma R\acute{6}(m',n')-\beta_{2n'}R\acute{8}(m',n'))R4(m',p)]\tilde{D}_p\}$$

$$+\sum_{m=1}^{M}\sum_{n'=1}^{N}\frac{\sin(\alpha_{2n'}t)}{\frac{(b-a)}{4}W(\omega\mu_o\gamma^2+\omega\varepsilon_o\beta_{2n'}^2)}[R5(m,n)R2(m,n')+R6(m,n)R4(m,n')]$$

$$\cdot\{\sum_{m'=1}^{M}\sum_{P=2}^{N}[(\omega\varepsilon_o\beta_{2n'}R\acute{5}(m',n')+\omega\mu_o\gamma R\acute{7}(m',n'))R1(m',p)$$

$$+(\omega\varepsilon_o\beta_{2n'}R\acute{6}(m',n')+\omega\mu_o\gamma R\acute{8}(m',n'))R3(m',p)]C_p$$

$$+\sum_{m'=1}^{M}\sum_{P=1}^{N}[(\omega\varepsilon_o\beta_{2n'}R\acute{5}(m',n')+\omega\mu_o\gamma R\acute{7}(m',n'))R2(m',p)$$

$$+(\omega\varepsilon_o\beta_{2n'}R\acute{6}(m',n')+\omega\mu_o\gamma R\acute{8}(m',n'))R4(m',p)]\tilde{D}_p\}$$

$$+\sum_{m=1}^{M}\sum_{n'=1}^{N}\{R5(m,n)R2(m,n')+R6(m,n)R4(m,n')\}\cos(\alpha_{2n'}t)\ \tilde{D}_{n'}$$

$$=\frac{(b-a)}{4}W(\omega\mu_o\gamma)\sin(\alpha_{2n}t)C_n+\frac{(\omega\mu_o\gamma)\cos(\alpha_{2n}t)}{(\omega\mu_o\gamma^2+\omega\varepsilon_o\beta_{2n}^2)}$$

$$\cdot\{\sum_{m=1}^{M}\sum_{n'=2}^{N}[(\gamma R\acute{5}(m,n)-\beta_{2n}R\acute{7}(m,n))R1(m,n')$$

$$+(\gamma R\acute{6}(m,n)-\beta_{2n}R\acute{8}(m,n))R3(m,n')]C_{n'}$$

$$+\sum_{m=1}^{M}\sum_{n'=1}^{N}[(\gamma R\acute{5}(m,n)-\beta_{2n}R\acute{7}(m,n))R2(m,n')$$

$$+\left(\gamma R_6'(m,n)-\beta_{2n}R_8'(m,n)\right)R4(m,n')\,]\tilde{D}_{n'}\}$$

$$+\frac{\beta_{2n}\cos(\alpha_{2n}t)}{(\omega\mu_o\gamma^2+\omega\varepsilon_o\beta_{2n}^2)}\{\sum_{m=1}^{M}\sum_{n'=2}^{N}[\left(\omega\varepsilon_o\beta_{2n}R_5'(m,n)+\omega\mu_o\gamma R_7'(m,n)\right)R1(m,n')$$

$$+\left(\omega\varepsilon_o\beta_{2n}R_6'(m,n)+\omega\mu_o\gamma R_8'(m,n)\right)R3(m,n')\,]C_{n'}$$

$$+\sum_{m=1}^{M}\sum_{n'=1}^{N}[\left(\omega\varepsilon_o\beta_{2n}R_5'(m,n)+\omega\mu_o\gamma R_7'(m,n)\right)R2(m,n')$$

$$+\left(\omega\varepsilon_o\beta_{2n}R_6'(m,n)+\omega\mu_o\gamma R_8'(m,n)\right)R4(m,n')\,]\tilde{D}_n\}$$

$$-\frac{(b-a)}{4}W(\alpha_{2n}\beta_{2n})\sin(\alpha_{2n}t)\;\tilde{D}_n \qquad \text{for } n:2\sim N \tag{A-1}$$

$$\sum_{m=1}^{M}\sum_{n'=2}^{N}\{R7(m,n)R1(m,n')+R8(m,n)R3(m,n')\}\cos(\alpha_{2n'}t)C_{n'}$$

$$-\sum_{m=1}^{M}\sum_{n'=2}^{N}\frac{\sin(\alpha_{2n'}t)}{\frac{(b-a)}{4}W(\omega\mu_o\gamma^2+\omega\varepsilon_o\beta_{2n'}^2)}\,[R7(m,n)R1(m,n')+R8(m,n)R3(m,n')\,]$$

$$\cdot\{\sum_{m'=1}^{M}\sum_{P=2}^{N}[\left(\gamma R_5'(m',n')-\beta_{2n'}R_7'(m',n')\right)R1(m',p)$$

$$+\left(\gamma R_6'(m',n')-\beta_{2n'}R_8'(m',n')\right)R3(m',p)\,]C_p$$

$$+\sum_{m'=1}^{M}\sum_{P=1}^{N}[\left(\gamma R_5'(m',n')-\beta_{2n'}R_7'(m',n')\right)R2(m',p)$$

$$+\left(\gamma R_6'(m',n')-\beta_{2n'}R_8'(m',n')\right)R4(m',p)\,]\;\tilde{D}_p\}$$

$$+\sum_{m=1}^{M}\sum_{n'=1}^{N}\frac{\sin(\alpha_{2n'}t)}{\frac{(b-a)}{4}W(\omega\mu_o\gamma^2+\omega\varepsilon_o\beta_{2n'}^2)}\,[R7(m,n)R2(m,n')+R8(m,n)R4(m,n')\,]$$

$$\cdot\{\sum_{m'=1}^{M}\sum_{P=2}^{N}[\left(\omega\varepsilon_o\beta_{2n'}R_5'(m',n')+\omega\mu_o\gamma R_7'(m',n')\right)R1(m',p)$$

$$+\left(\omega\varepsilon_o\beta_{2n'}R_6'(m',n')+\omega\mu_o\gamma R_8'(m',n')\right)R3(m',p)\,]C_p$$

$$+\sum_{m'=1}^{M}\sum_{P=1}^{N}\left[\left(\omega\varepsilon_o\beta_{2n'}R_5'(m',n')+\omega\mu_o\gamma R_7'(m',n')\right)R2(m',p)\right.$$

$$\left.+\left(\omega\varepsilon_o\beta_{2n'}R_6'(m',n')+\omega\mu_o\gamma R_8'(m',n')\right)R4(m',p)\right]\tilde{D}_p\Big\}$$

$$+\sum_{m=1}^{M}\sum_{n'=1}^{N}\left\{R7(m,n)R2(m,n')+R8(m,n)R4(m,n')\right\}\cos(\alpha_{2n'}t)C_{n'}$$

$$=\frac{(b-a)}{4}W(\omega\mu_o\beta_{2n})\sin(\alpha_{2n}t)C_n+\frac{(\omega\mu_o\beta_{2n})\cos(\alpha_{2n}t)}{\omega\mu_o\gamma^2+\omega\varepsilon_o\beta_{2n}^2}$$

$$\cdot\Big\{\sum_{m=1}^{M}\sum_{n'=2}^{N}\left[\left(\gamma R_5'(m,n)-\beta_{2n}R_7'(m,n)\right)R1(m,n')\right.$$

$$\left.+\left(\gamma R_6'(m,n)-\beta_{2n}R_8'(m,n)\right)R3(m,n')\right]C_{n'}$$

$$+\sum_{m=1}^{M}\sum_{n'=1}^{N}\left[\left(\gamma R_5'(m,n)-\beta_{2n}R_7'(m,n)\right)R2(m,n')\right.$$

$$\left.+\left(\gamma R_6'(m,n)-\beta_{2n}R_8'(m,n)\right)R4(m,n')\right]\tilde{D}_{n'}\Big\}$$

$$-\frac{\gamma(1+\delta_n^1)\cos(\alpha_{2n}t)}{(\omega\mu_o\gamma^2+\omega\varepsilon_o\beta_{2n}^2)}\Big\{\sum_{m=1}^{M}\sum_{n'=2}^{N}\left[\left(\omega\varepsilon_o\beta_{2n}R_5'(m,n)+\omega\mu_o\gamma R_7'(m,n)\right)R1(m,n')\right.$$

$$\left.+\left(\omega\varepsilon_o\beta_{2n}R_6'(m,n)+\omega\mu_o\gamma R_8'(m,n)\right)R3(m,n')\right]C_{n'}$$

$$+\sum_{m=1}^{M}\sum_{n'=1}^{N}\left[\left(\omega\varepsilon_o\beta_{2n}R_5'(m,n)+\omega\mu_o\gamma R_7'(m,n)\right)R2(m,n')\right.$$

$$\left.+\left(\omega\varepsilon_o\beta_{2n}R_6'(m,n)+\omega\mu_o\gamma R_8'(m,n)\right)R4(m,n')\right]\tilde{D}_{n'}\Big\}$$

$$+\frac{(b-a)}{4}W\gamma\alpha_{2n}(1+\delta_n^1)\sin(\alpha_{2n}t)\,\tilde{D}_n \qquad \text{for n: 1~N} \qquad \text{(A-2)}$$

where δ_n^1 is the Kronecker delta function,

$$\delta_n^1=\begin{cases}1 & \text{if } n=1\\ 0 & \text{otherwise}\end{cases} \qquad \text{(A-3)}$$

$$R1(m,n) = \frac{1}{\varepsilon_{R2}}\,\alpha_{2n}\left(\beta_m A_{sc}(m,n)\beta_{2n} - B_{cs}(m,n)\gamma^2\right) \tag{A-4}$$

$$R2(m,n) = \omega\varepsilon_o\gamma\left(\beta_m A_{sc}(m,n)+\beta_{2n}B_{cs}(m,n)\right) \tag{A-5}$$

$$R3(m,n) = \frac{1}{\varepsilon_{R2}}\,\alpha_{2n}\gamma\left(\beta_{2n}A_{sc}(m,n)+\beta_m B_{cs}(m,n)\right) \tag{A-6}$$

$$R4(m,n) = \omega\varepsilon_o\left(A_{sc}(m,n)\gamma^2 - \beta_m\beta_{2n}B_{cs}(m,n)\right) \tag{A-7}$$

$$R5(m,n) = (\omega\mu_o\gamma)B_{cs}(m,n)\varepsilon_{R1}/\alpha_{1m}/(\beta_m^2+\gamma^2) \tag{A-8}$$

$$R6(m,n) = \alpha_{1m}\beta_m B_{cs}(m,n)/\omega\varepsilon_o/(\beta_m^2+\gamma^2) \tag{A-9}$$

$$R7(m,n) = -\omega\mu_o\varepsilon_{R1}\beta_m A_{sc}(m,n)/\alpha_{1m}/(\beta_m^2+\gamma^2) \tag{A-10}$$

$$R8(m,n) = \gamma\alpha_{1m}A_{sc}(m,n)/\omega\varepsilon_o/(\beta_m^2+\gamma^2) \tag{A-11}$$

$$R5'(m,n) = -(\omega\mu_o\gamma)B_{cs}(m,n)\varepsilon_{R3}\cdot P_E(m)/\alpha_{3m}/(\beta_m^2+\gamma^2) \tag{A-12}$$

$$R6'(m,n) = -\alpha_{3m}\beta_m B_{cs}(m,n)/(\omega\varepsilon_o)/(\beta_m^2+\gamma^2)/P_F(m) \tag{A-13}$$

$$R7'(m,n) = -\omega\mu_o\beta_m\varepsilon_{R3}A_{sc}(m,n)/\alpha_{3m}/(\beta_m^2+\gamma^2) \tag{A-14}$$

$$R8'(m,n) = \alpha_{3m}\gamma A_{sc}(m,n)/\omega\varepsilon_o/(\beta_m^2+\gamma^2)/P_F(m) \tag{A-15}$$

$$P_E(m) = \tilde{E}_m/E_m \tag{A-16}$$

$$P_F(m) = \tilde{F}_m/F_m \tag{A-17}$$

$$A_{sc}(m,n) = -\frac{\cos(\beta_{2n}a)}{2}\left\{\frac{\cos[(\beta_m-\beta_{2n})x]}{\beta_m-\beta_{2n}}+\frac{\cos[(\beta_m+\beta_{2n})x]}{\beta_m+\beta_{2n}}\right\}_{x=a}^{x=b} + \frac{\sin(\beta_{2n}a)}{2}\left\{\frac{\sin[(\beta_m-\beta_{2n})x]}{\beta_m-\beta_{2n}}-\frac{\sin[(\beta_m+\beta_{2n})x]}{\beta_m+\beta_{2n}}\right\}_{x=a}^{x=b} \tag{A-18}$$

$$B_{cs}(m,n) = -\frac{\cos(\beta_{2n}a)}{2}\left\{-\frac{\cos[(\beta_n-\beta_{2n})x]}{\beta_m-\beta_{2n}}+\frac{\cos[(\beta_m+\beta_{2n})x]}{\beta_m+\beta_{2n}}\right\}_{x=a}^{x=b} - \frac{\sin(\beta_{2n}a)}{2}\left\{\frac{\sin[(\beta_m-\beta_{2n})x]}{\beta_m-\beta_{2n}}+\frac{\sin[(\beta_m+\beta_{2n})x]}{\beta_m+\beta_{2n}}\right\}_{x=a}^{x=b} \tag{A-19}$$

References

[1] C.P. Lee, P.L. Miller, D. Hou, and R.J. Anderson,'Ultra high spped integrated circuits using GaAs/GaAlAs high mobility transistors,'in Proc. Device Research Conf. IIA-7, June 1983.

[2] R.K. Jain, K. Stenersen, D.E. Snyder,'Picosecond optoelectronics in high-speed integrated circuits', Proceedings of SPIE, Vol. 439, pp. 174-176, 1983.

[3] H. Hasegawa, S. Seki,'Analysis of interconnection delay on very high-speed LSI/VLSI chips using an microstrip line model,'IEEE Trans. Microwave Theory and Tech., vol. MTT-32, no. 12, pp. 1721-1727, Dec. 1984.

[4] M. Riaziat,I. Zubeck,S. Bandy, and G. Zdasiuk,'Coplanar waveguides used in 2-18 GHz distributed amplifier,'IEEE MTT-S International Microwave Symposium, pp. 337-338, June 1986.

[5] R.W. Jackson, 'Coplanar Waveguide vs. microstrip for millimeter wave integrated circuits,'IEEE MTT-S International Microwave Symposium , pp. 699-702, June 1986.

[6] H. Hasegawa and H. Okizaki,'M.I.S. and Schottky slow-wave coplanar stripline on GaAs substrate,'Electron. Lett., vol. 13, pp.663-664, Oct. 1977.

[7] Y. Fukuoka, Y. C. Shih, and T. Itoh,'Analysis of slow-wave coplanar waveguide for monolithic integrated circuits,'IEEE Trans. Microwave Theory Tech., vol. MTT-31, no.7, pp.567-573, July 1983.

[8] K. K. Li, G. Arjavalingam, A. Dienes, and J. R. Whinnery,'Propagation of picosecond pulses on microwave striplines,'IEEE Trans. Microwave Theory and Tech., vol. MTT-30, no. 8, pp.1270-1273, August 1982.

[9] G. Hasnain, A. Dienes, and J. R. Whinnery,'Dispersion of picosecond pulses in coplanar transmission lines,'IEEE Trans. Microwave Theory and Tech., vol. MTT-34, no. 6, pp. 738-741, June 1986.

[10] R. L. Veghte and C. A. Balanis,'Dispersion of transient signals in microstrip transmission lines,'IEEE MTT-S International Microwave Symposium digest, pp. 691-694, June 1986.

[11] C.Seguinot, P.Kennis, P.Pribetich, J.F.Legier,'Crosstalk phenomenon in coupled microstrip lines laid on semi-conducting substrates,'15th European Microwave Conference Digest, pp. 826-830, Paris, Sep. 1985.

[12] C-K Tzuang and T. Itoh,'Pulse transmission on a slow-wave MIS and Schottky coplanar waveguide with finite conductor thickness,'15th European Microwave Conference Digest , pp.

225-230, Paris, France, Sep. 1985.

[13] C-K Tzuang and T. Itoh,'Pulse transmission in an interconnection line on a semiconductor substrate with a lossy layer,'1985 VLSI Multilevel Interconnection Conference Digest, pp.424-430 June 25-26, Santa Clara, CA.

[14] R. Mittra, Y. L. Hou, and V. Jamnejad,'Analysis of open dielectric waveguides using mode-matching technique and variational methods,'IEEE Trans. Microwave Theory and Tech., vol. MTT-28, pp. 36-43, Jan. 1980.

[15] G. Kowalski and R. Pregla,'Dispersion characteristics of shielded microstrips with finite thickness,'Arch. Elek. Ubertragung, vol. 25, no. 4, pp.193-196, April 1971.

[16] Sze,'Physics of Semiconductor Devices,'pp.33, 2nd edition, 1981, John Wiley & Sons, Inc.

[17] H. Ogawa and T. Itoh,'Slow-wave characteristics of ferromagnetic semiconductor microstrip lines,'IEEE MTT-S International Microwave Symposium Digest,pp.65-68, June 1986.

END

1-87

DTIC